Pressure-Induced Excitations in the Out-of-Plane Optical Response of the Nodal-Line Semimetal ZrSiS

J. Ebad-Allah,[1,2] S. Rojewski,[1] M. Vöst,[3] G. Eickerling,[3] W. Scherer,[3] E. Uykur,[4] Raman Sankar,[5] L. Varrassi,[6] C. Franchini,[7,6] K.-H. Ahn,[8,10] J. Kuneš,[8,9] and C. A. Kuntscher[1,*]

[1]*Experimentalphysik II, University of Augsburg, 86159 Augsburg, Germany*
[2]*Department of Physics, Tanta University, 31527 Tanta, Egypt*
[3]*Chair of Chemical Physics and Materials Science, Institute of Physics, University of Augsburg, 86159 Augsburg, Germany*
[4]*1. Physikalisches Institut, Universität Stuttgart, 70569 Stuttgart, Germany*
[5]*Institute of Physics, Academia Sinica, Taipei 11529, Taiwan*
[6]*Department of Physics and Astronomy, Alma Mater Studiorum-Università di Bologna, Bologna 40127, Italy*
[7]*University of Vienna, Faculty of Physics and Center for Computational Materials Science, 1090 Vienna, Austria*
[8]*Institute of Solid State Physics, TU Wien, 1020 Vienna, Austria*
[9]*Institute of Physics, The Czech Academy of Sciences, 18221 Praha, Czechia*
[10]*Institute of Physics, The Czech Academy of Sciences, 16200 Praha, Czechia*

(Received 8 March 2021; accepted 17 June 2021; published 11 August 2021)

The anisotropic optical response of the layered, nodal-line semimetal ZrSiS at ambient and high pressure is investigated by frequency-dependent reflectivity measurements for the polarization along and perpendicular to the layers. The highly anisotropic optical conductivity is in very good agreement with results from density-functional theory calculations and confirms the anisotropic character of ZrSiS. Whereas the in-plane optical conductivity shows only modest pressure-induced changes, we found strong effects on the out-of-plane optical conductivity spectrum of ZrSiS, with the appearance of two prominent excitations. These pronounced pressure-induced effects can neither be attributed to a structural phase transition according to our single-crystal x-ray diffraction measurements, nor can they be explained by electronic correlation and electron-hole pairing effects, as revealed by theoretical calculations. Our findings are discussed in the context of the recently proposed excitonic insulator phase in ZrSiS.

DOI: 10.1103/PhysRevLett.127.076402

Topological nodal-line semimetals (NLSMs) with linearly dispersing electronic bands, which cross along a line in reciprocal space, host two-dimensional (2D) Dirac fermions and are currently extensively investigated due to their exotic and highly interesting physical properties [1,2]. The layered material ZrSiS is considered as the prototype NLSM, where the linearly dispersing bands extend over a large energy range ∼2 eV around the Fermi energy E_F, without the presence of topologically trivial bands in the vicinity of E_F, and the corresponding nodal lines form a three-dimensional cagelike structure [3–6]. There are additional Dirac crossings at the X and R point of the Brillouin zone located ∼0.5 eV above and below E_F, which are protected by nonsymmorphic symmetry against gapping due to the spin-orbit coupling. The unconventional mass enhancement of quasiparticles in ZrSiS [6] suggests the importance of electronic correlations, which could potentially drive the material toward an excitonic insulator phase or a quantum critical region close to it [7–9].

The exceptional electronic band structure of ZrSiS and related materials ZrXY, where X is a carbon group element (X = Si, Ge, Sn) and Y is a chalcogen element (Y = S, Se, Te) [10], is mainly due to the 2D square nets of Si atoms parallel to the ab plane, which are the main structural motif besides the square nets of Zr and chalcogen atoms, stacked perpendicular to the ab plane [see inset of Fig. 1(b)]. Further interesting properties of ZrSiS include high charge carrier mobility and exceptionally large magnetoresistance due to electron-hole symmetry [11–13]. Also, the electrodynamic properties of ZrSiS are unusual, with a nearly frequency-independent optical conductivity σ_1 for frequencies from 250 to 2500 cm^{-1} (30–300 meV) [14]. This rather flat behavior of σ_1 is followed by a U-shaped profile between 3000 and 10 000 cm^{-1} (0.37–1.24 eV), which was ascribed to transitions between the linearly crossing bands of the nodal line close to E_F, and a peak located at ∼11 800 cm^{-1} (∼1.46 eV), associated with transitions between parallel bands of the Dirac crossings protected by nonsymmorphic symmetry [15].

All previous experimental studies on the electrodynamic properties of ZrSiS focused on the in-plane optical response, i.e., for the polarization **E** of the incident electromagnetic radiation aligned along the layers in the ab plane [see inset of Fig. 1(b)]. In this Letter, we report on the out-of-plane optical conductivity of ZrSiS, as obtained by frequency-dependent reflectivity measurements for **E**

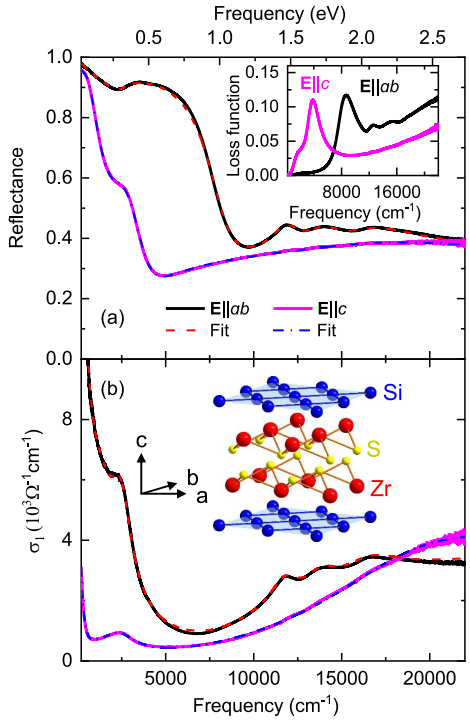

FIG. 1. Optical response functions of ZrSiS at ambient conditions for polarization directions $\mathbf{E}\|ab$ and $\mathbf{E}\|c$: (a) reflectivity spectra and (b) real part of the optical conductivity σ_1. Inset of (a): loss function $-\mathrm{Im}(1/\hat{\epsilon})$, where $\hat{\epsilon}$ is the complex dielectric function. Inset of (b): crystal structure of ZrSiS with Si square nets parallel to the ab plane.

directed perpendicular to the layers, i.e., $\mathbf{E}\|c$. Furthermore, we studied the in-plane and out-of-plane optical conductivity of ZrSiS under external, quasihydrostatic pressure, combined with pressure-dependent single-crystal x-ray diffraction (XRD) measurements. In the out-of-plane optical response, two new excitations appear under pressure, which cannot be reproduced by density-functional theory (DFT) calculations at the generalized gradient approximation [16] level or even by including electronic correlations at GW level and electron-hole pairing effects. Our findings add yet another interesting facet to the exceptional properties of ZrSiS.

Ambient-pressure reflectivity spectra of ZrSiS for the polarization along ($\mathbf{E}\|ab$) and perpendicular ($\mathbf{E}\|c$) to the layers are depicted in Fig. 1(a). (See the Supplemental Material [17] for a description of sample preparation, experimental details, and analysis of reflectivity data.) For both polarization directions, the reflectivity is high at low energies and shows a distinct plasma edge, indicating the metallic character consistent with recent resistivity measurements [38,39]. The anisotropic character of ZrSiS is manifested by the polarization-dependent energy position of the plasma edge, which is shifted toward lower energies for $\mathbf{E}\|c$ compared to $\mathbf{E}\|ab$. Consistently, the intraband plasmon peak in the loss function defined as $-\mathrm{Im}(1/\hat{\epsilon})$, where $\hat{\epsilon}$ is the complex dielectric function, appears at lower energy, $\approx$0.47 eV, for $\mathbf{E}\|c$ as compared to $\approx$1.07 eV for $\mathbf{E}\|ab$ [inset of Fig. 1(a)]. The anisotropic optical response is also seen in the real part of the optical conductivity spectrum σ_1, displayed in Fig. 1(b). For both directions, σ_1 consists of a Drude term at low energies due to itinerant charge carriers. From the spectral weight analysis of the Drude contribution, we obtain a plasma frequency ω_p of 3.17 eV for $\mathbf{E}\|ab$ and 1.08 eV for $\mathbf{E}\|c$, in agreement with the results of first-principles calculations [40]. The ratio of dc conductivities σ_{ab}/σ_c amounts to $\sim$16, i.e., it falls in the 8–30 range reported in previous studies [38,39], respectively. Obviously, the intra-layer charge transport dominates over the inter-layer one.

Also, the profile of the optical conductivity spectrum is strongly polarization dependent [Fig. 1(b)], in very good agreement with the theoretical results of Refs. [39,41]. For $\mathbf{E}\|ab$, the low-energy σ_1 spectrum consists of a Drude term and a rather flat region up to $\sim$3000 cm^{-1} followed by a U-shape frequency dependence, which is bounded by a rather sharp peak at high frequencies [14,15]. This sharp peak (called $L4$ in the following) is associated with transitions between parallel bands of the Dirac crossings, which are protected by nonsymmorphic symmetry against gapping [15]. The profile of the $\mathbf{E}\|c$ optical conductivity is markedly different: It is rather featureless, namely, besides the Drude peak it shows only an absorption peak at $\sim$2400 cm^{-1} and a monotonic increase above $\sim$6000 cm^{-1}, which originates from transitions between Dirac bands and states further away from E_F. Compared to $\mathbf{E}\|ab$, the out-of plane momentum matrix elements exhibit substantially weaker $k-$ and band dependence, and thus the $\mathbf{E}\|c$ optical conductivity reflects the behavior of the particle-hole (joint) density of states (divided by frequency) [15]. For both directions, the optical conductivity and reflectivity spectra can be well fitted with the Drude-Lorentz model (see Fig. 1). The obtained Drude and Lorentz contributions at ambient pressure are shown in Figs. 2(a) and 2(b) for $\mathbf{E}\|ab$ and $\mathbf{E}\|c$, respectively. For comparison with the results of DFT calculations (see the Supplemental Material [17] for details), we subtracted the Drude term from the total σ_1 spectrum and obtained the contributions from the interband transitions $\sigma_{1,\mathrm{interband}}$. The interband conductivity spectra agree well with the corresponding theoretical spectra [see inset of Fig. 2(a)].

In the following, the main focus will be on the optical response of ZrSiS under external pressure. The experimental in-plane and out-of-plane σ_1 spectra are depicted for selected pressures in Figs. 2(a) and 2(b), respectively. First, we discuss the results for the in-plane optical response. One notices that the induced changes for $\mathbf{E}\|ab$ are only modest, and the characteristic profile of the optical conductivity with its U-shape is unchanged up to 7 GPa. A detailed analysis reveals a slight increase of σ_1 below $\sim$3000 cm^{-1} and a shift of the $L4$ peak to higher energies with increasing pressure. A comparison between the experimental and

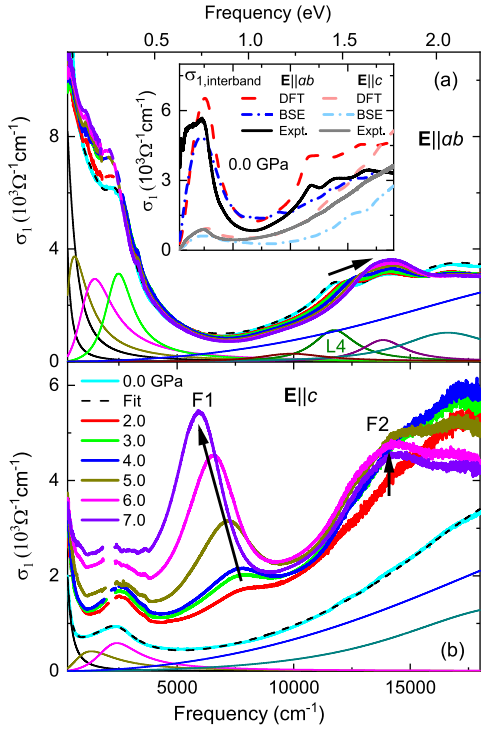

FIG. 2. Pressure-dependent optical conductivity σ_1 with the Drude-Lorentz fitting and the corresponding contributions at 0 GPa for (a) $\mathbf{E}\|ab$ and (b) $\mathbf{E}\|c$. Arrows mark the most pronounced pressure-induced changes in the spectra. Inset of (a): comparison between the experimental and both DFT and BSE calculated interband conductivity $\sigma_{1,\mathrm{interband}}$ at 0 GPa.

theoretical interband optical conductivity from DFT calculations for $\mathbf{E}\|ab$ is given in Fig. 3(a) for two selected pressures (2.0 and 7.0 GPa). Similar to the experimental spectra, the U-shape of the theoretical spectrum is retained up to the highest measured pressure and the $L4$ peak at the high-energy bound of the U-shape is blueshifted. According to the behavior of the $L4$ peak, pressure induces a shift of the nonsymmorphic symmetry protected Dirac crossings *away* from E_F, as a result of the compression of the crystal lattice.

Consistently, the thermal contraction of the crystal lattice during cooling causes a blueshift of the $L4$ peak [see Fig. 3(c)] [42]. A comparison between the effect of cooling and pressure on the energy position of the $L4$ peak is given in Fig. 3(d), whereby for the latter both experimental and DFT results are displayed [43]. To conclude, tensile strain, instead of compressive strain, would be needed to push the nonsymmorphic symmetry protected Dirac nodes in ZrSiS *toward* E_F, in order to study the expected distinct physics related to these 2D Dirac fermions [45].

Next, we will discuss the pressure-induced effects on the out-of-plane optical conductivity [see Fig. 2(b)]. Starting from the lowest applied pressure (2 GPa), drastic changes occur in the profile of the $\mathbf{E}\|c$ σ_1 spectrum: in addition to the pressure-induced increase below ~5000 cm^{-1}, two new excitations labeled $F1$ and $F2$ appear, which gain spectral weight with increasing pressure [46]. Similar to the in-plane optical response, a Drude-Lorentz model was applied for fitting the experimental spectra. As an example, we depict in Fig. 3(b) the experimental interband conductivity $\sigma_{1,\mathrm{interband}}$ at 7 GPa, where the Drude term was subtracted from the total σ_1, together with the Lorentz contributions. Each of the two new excitations $F1$ and $F2$ can be well described by one Lorentzian term. With increasing pressure, the energy position of excitation $F2$ is almost unchanged, whereas $F1$ first shifts slightly to lower energies for pressures up to ~4 GPa, and for pressures above 4 GPa, this redshift gets more pronounced [Fig. 3(e)]. The oscillator strength of $F1$ and $F2$ slightly increases with increasing pressure up to 4 GPa and increases strongly above ~4 GPa [inset of Fig. 3(e)] due to a transfer of spectral weight from the energy range above ~1.9 eV. In Fig. 3(b), we compare the experimental $\mathbf{E}\|c$ $\sigma_{1,\mathrm{interband}}$ spectrum for two selected pressures, 2.0 and 7.0 GPa, with the corresponding DFT results. Interestingly, the theoretical interband conductivity for $\mathbf{E}\|c$ is basically unchanged upon pressure application, in strong contrast to the experimental results. In particular, the two excitations $F1$ and $F2$ are *not* reproduced in the pressure-dependent theoretical spectra. Thus, the excitations $F1$ and $F2$ should be attributed to effects that are not included in the band structure calculations, and hence the role of beyond-DFT effects might be relevant, as discussed below.

For an interpretation of our findings, we performed a high-pressure XRD study on a ZrSiS single crystal (see the Supplemental Material [17] for details). With increasing pressure, the lattice parameters a and c monotonically decrease, resulting in a monotonic volume decrease [see Fig. 3(f)]. Further investigation of the reciprocal space up to maximum measured pressure (6.9 GPa) does not reveal the formation of additional or superstructural Bragg reflections [17]. Hence, our diffraction data do not provide any hint for a structural phase transition up to at least ~7 GPa, in agreement with Refs. [47,48]. This finding is in contradiction with results of powder XRD experiments, which suggested a structural phase transition at elevated pressures [44]. We fitted the volume V with the second-order Murnaghan equation of state (EOS) [49] according to $V(p) = V_0 \cdot [(B_0'/B_0) \cdot p + 1]^{-1/B_0'}$, where B_0 is the bulk modulus, B_0' is its pressure derivative, which is fixed to 4, and V_0 is the volume, all at $P = 0$ GPa. From the fitting, we obtain the value $B_0 = 144 \pm 5$ GPa, consistent with earlier reports [44,50].

Based on the results of our high-pressure XRD study, we can discuss the optical data in more detail. First, it has been proposed that the distance of the nonsymmorphic Dirac crossings from E_F is inversely proportional to the distance between the Si atoms in the Si-Si square nets [51] and hence inversely proportional to the lattice parameter a. Accordingly, the energy position of the related $L4$ peak in

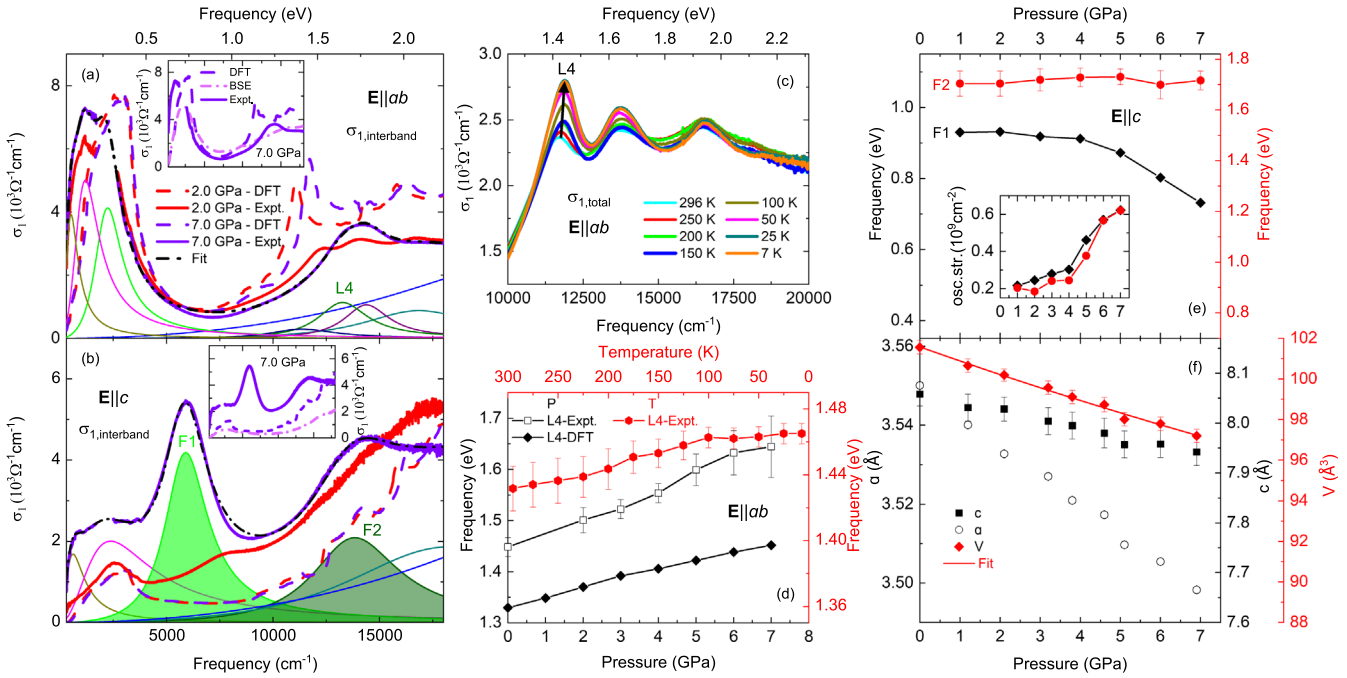

FIG. 3. (a),(b) Comparison between the experimental and DFT interband conductivity $\sigma_{1,\text{interband}}$ at 2.0 and 7.0 GPa, with the total fitting curve and the fitting contributions for the experimental $\sigma_{1,\text{interband}}$ at 7.0 GPa, for $\mathbf{E}\|ab$ and $\mathbf{E}\|c$, respectively. Insets of (a),(b): comparison between DFT and BSE theoretical results and experimental interband conductivity σ_1 at 7.0 GPa for $\mathbf{E}\|ab$ and $\mathbf{E}\|c$, respectively. (c) Temperature-dependent high-energy optical conductivity for $\mathbf{E}\|ab$. The arrow marks the temperature-induced shift of the $L4$ peak. (d) Comparison between the temperature (T) and pressure (P) dependence (both experimental and theoretical) of the frequency position of the $L4$ peak. (e) Pressure-dependent frequency position and oscillator strength (osc. str., inset) of the peaks $F1$ and $F2$. (f) Volume V of the unit cell and lattice parameters a and b as a function of pressure. The error bars represent three times the estimated standard deviation. The solid line is a fit with a Murnaghan-type EOS (see text).

the $\mathbf{E}\|ab$ σ_1 spectrum should scale with $1/a$. However, based on our pressure-dependent optical data, we cannot confirm such a behavior. Second, the experimental optical data show an anomaly at ≈4 GPa in the shift of the $F1$ excitation and in the oscillator strength of the $F1$ and $F2$ excitations. Since our pressure-dependent XRD results do not provide any evidence for a structural phase transition, this anomaly arises from purely electronic behavior, like in pressurized ZrSiTe [52,53]. The origin of the excitations $F1$ and $F2$, which appear under pressure in the experimental $\mathbf{E}\|c$ optical conductivity, remains, however, unclear.

It is interesting to note that, based on calculations for a bilayer square lattice model, Rudenko *et al.* [7] suggested that ZrSiS undergoes a condensation of interlayer zero-momentum excitons due to electronic correlations and a high degree of electron-hole symmetry of the electronic band structure, which gives rise to an excitonic insulator state at low temperature. In this weak-coupling scenario (formally similar to BCS superconductivity), a gap opens at E_F in the excitonic insulator state, which leads to a spectral weight transfer and appearance of Hebel-Slichter–like peaks [7,54]. Transitions between these peaks could, in principle, lead to distinct excitations in the conductivity spectrum [55]. However, the signatures of the exciton instability have not been experimentally observed in ZrSiS until now, in particular, no pseudogap was observed in photoemission spectra. The observation that the $F1$ peak draws its spectral weight from the high- rather than the low-energy part of the spectrum also contradicts this scenario.

To inspect the role of zero-momentum excitons in the formation of the $F1$ and $F2$ peaks, we have computed the interband optical spectra by solving the Bethe-Salpeter equation (BSE) with quasiparticle energies calculated at GW level, also testing the impact of the coupling between the resonant and antiresonant excitations. The results, depicted in the insets of Figs. 2(a), 3(a), and 3(b), show that the optical conductivity is only marginally affected by the electronic correlation and excitonic effects: the BSE σ_1 spectra are very similar to the DFT spectra and do not exhibit any evident pressure dependence. Formation of a single exciton thus cannot explain our experimental results. A more complex possibility would be the creation of a finite-momentum exciton accompanied by a phonon or another exciton, in order to ensure the momentum conservation. A first step in analysis of such a scenario would be extending the BSE analysis to finite-momentum transfer.

Another scenario was proposed recently [9], suggesting that ZrSiS should be located in a quantum critical region between the NLSM and excitonic insulator phases, which could explain the observed quasiparticle mass

enhancement [6] in the absence of a pseudogap, consistent with reported photoemission spectra and our optical data. Nevertheless, both the excitonic insulator and quantum critical scenarios are at odds with our observation of pressure-insensitive in-plane response σ_{ab} and with our theoretical predictions. We note that a purely electronic excitonic insulator phase with permanent out-of-plane electric dipole moments arranged in an antiferroelectric pattern was recently proposed in bulk MoS_2 under pressure [56], which might be relevant for pressurized ZrSiS as well.

In conclusion, according to our reflectivity study, the optical response of the NLSM ZrSiS is highly anisotropic. The polarization-dependent optical conductivity at ambient pressure is in very good agreement with the results of DFT calculations. The in-plane optical response shows only modest changes under pressure, consistent with theoretical predictions. In stark contrast, the out-of-plane optical conductivity undergoes strong changes under pressure, with the appearance of two pronounced peaks. The observed pressure-induced changes can neither be attributed to a structural phase transition according to our single-crystal XRD data, nor can they be explained by electronic correlation effects and single exciton formation according to our theoretical calculations.

We thank S. Sharma for fruitful discussions. C. A. K. acknowledges financial support from the Deutsche Forschungsgemeinschaft (DFG), Germany, through Grant No. KU 1432/13-1. R. S. acknowledges financial support provided by the Ministry of Science and Technology in Taiwan under Projects No. MOST-108-2112-M-001-049-MY2, No. 110-2112-M-001-065-MY3 and acknowledges Academia Sinica for the budget of AS-iMATE-109-13.

*christine.kuntscher@physik.uni-augsburg.de

[1] A. A. Burkov and L. Balents, Weyl Semimetal in a Topological Insulator Multilayer, Phys. Rev. Lett. **107**, 127205 (2011).

[2] C. Fang, Y. Chen, H.-Y. Kee, and L. Fu, Topological nodal line semimetals with and without spin-orbital coupling, Phys. Rev. B **92**, 081201(R) (2015).

[3] L. M. Schoop, M. N. Ali, C. Strasser, V. Duppel, S. S. P. Parkin, B. V. Lotsch, and C. R. Ast, Dirac cone protected by non-symmorphic symmetry and three-dimensional Dirac line node in ZrSiS, Nat. Commun. **7**, 11696 (2016).

[4] M. Neupane, I. Belopolski, M. M. Hosen, D. S. Sanchez, R. Sankar, M. Szlawska, S.-Y. Xu, K. Dimitri, N. Dhakal, P. Maldonado, P. M. Oppeneer, D. Kaczorowski, F. Chou, M. Z. Hasan, and T. Durakiewicz, Observation of topological nodal fermion semimetal phase in ZrSiS, Phys. Rev. B **93**, 201104(R) (2016).

[5] C. Chen *et al.*, Dirac line nodes and effect of spin-orbit coupling in the nonsymmorphic critical semimetals MSiS (M = Hf, Zr), Phys. Rev. B **95**, 125126 (2017).

[6] S. Pezzini, M. R. van Delft, L. Schoop, B. Lotsch, A. Carrington, M. I. Katsnelson, N. E. Hussey, and S. Wiedmann, Unconventional mass enhancement around the Dirac nodal loop in ZrSiS, Nat. Phys. **14**, 178 (2018).

[7] A. N. Rudenko, E. A. Stepanov, A. I. Lichtenstein, and M. I. Katsnelson, Excitonic Instability and Pseudogap Formation in Nodal Line Semimetal ZrSiS, Phys. Rev. Lett. **120**, 216401 (2018).

[8] M. M. Scherer, C. Honerkamp, A. N. Rudenko, E. A. Stepanov, A. I. Lichtenstein, and M. I. Katsnelson, Excitonic instability and unconventional pairing in the nodal-line materials ZrSiS and ZrSiSe, Phys. Rev. B **98**, 241112(R) (2018).

[9] J.-R. Wang, G.-Z. Liu, X. Wan, and C. Zhang, Quantum criticality of the excitonic insulating transition in the nodal-line semimetal ZrSiS, Phys. Rev. B **101**, 245151 (2020).

[10] C. Wang and T. Hughbanks, Main group element size and substitution effects on the structural dimensionality of zirconium tellurides of the ZrSiS type, Inorg. Chem. **34**, 5524 (1995).

[11] R. Sankar, G. Peramaiyan, I. P. Muthuselvam, C. J. Butler, K. Dimitri, M. Neupane, G. N. Rao, M.-T. Lin, and F. C. Chou, Crystal growth of Dirac semimetal ZrSiS with high magnetoresistance and mobility, Sci. Rep. **7**, 40603 (2017).

[12] Y.-Y. Lv, B.-B. Zhang, X. Li, S.-H. Yao, Y. B. Chen, J. Zhou, S.-T. Zhang, M.-H. Lu, and Y.-F. Chen, Extremely large and significantly anisotropic magnetoresistance in ZrSiS single crystals, Appl. Phys. Lett. **108**, 244101 (2016).

[13] R. Singha, A. K. Pariari, B. Satpati, and P. Mandal, Large nonsaturating magnetoresistance and signature of nondegenerate Dirac nodes in ZrSiS, Proc. Natl. Acad. Sci. U.S.A. **114**, 2468 (2017).

[14] M. B. Schilling, L. M. Schoop, B. V. Lotsch, M. Dressel, and A. V. Pronin, Flat Optical Conductivity in ZrSiS Due to Two-Dimensional Dirac Bands, Phys. Rev. Lett. **119**, 187401 (2017).

[15] J. Ebad-Allah, J. F. Afonso, M. Krottenmüller, J. Hu, Y. L. Zhu, Z. Q. Mao, J. Kuneš, and C. A. Kuntscher, Chemical pressure effect on the optical conductivity of the nodal-line semimetals ZrSiY (Y = S, Se, Te) and ZrGeY (Y = S, Te), Phys. Rev. B **99**, 125154 (2019).

[16] J. P. Perdew, K. Burke, and M. Ernzerhof, Generalized Gradient Approximation Made Simple, Phys. Rev. Lett. **77**, 3865 (1996).

[17] See Supplemental Material at http://link.aps.org/supplemental/10.1103/PhysRevLett.127.076402 for details about sample preparation, polarization-dependent reflectivity measurements at ambient and high pressure, analysis of reflectivity and optical conductivity spectra, XRD measurements under pressure, and theoretical calculations, which includes Refs. [18–37].

[18] W. Bensch, O. Helmer, M. Muhler, H. Ebert, and M. Knecht, Experimental and theoretical bandstructure of the layer compound ZrSiTe, J. Phys. Chem. **99**, 3326 (1995).

[19] H. K. Mao, J. Xu, and P. M. Bell, Calibration of the ruby pressure gauge to 800 kbar under quasi-hydrostatic conditions, J. Geophys. Res. **91**, 4673 (1986).

[20] K. Syassen, Ruby under pressure, High Press. Res. **28**, 75 (2008).

[21] M. I. Eremets and Y. A. Timofeev, Miniature diamond anvil cell: Incorporating a new design for anvil alignment, Rev. Sci. Instrum. **63**, 3123 (1992).

[22] L. Merrill and W. A. Bassett, Miniature diamond anvil pressure cell for single crystal x-ray diffraction studies, Rev. Sci. Instrum. **45**, 290 (1974).
[23] R. Boehler and K. De Hantsetters, New anvil designs in diamond-cells, High Press. Res. **24**, 391 (2004).
[24] S. A. Moggach, D. R. Allan, S. Parsons, and J. E. Warren, Incorporation of a new design of backing seat and anvil in a Merrill-Bassett diamond anvil cell, J. Appl. Crystallogr. **41**, 249 (2008).
[25] G. J. Piermarini, S. Block, J. D. Barnett, and R. A. Forman, Calibration of the pressure dependence of the R1 ruby fluorescence line to 195 kbar, J. Appl. Phys. **46**, 2774 (1975).
[26] A. Dewaele, M. Torrent, P. Loubeyre, and M. Mezouar, Compression curves of transition metals in the Mbar range: Experiments and projector augmented-wave calculations, Phys. Rev. B **78**, 104102 (2008).
[27] I. Kantor, Fluorescense pressure calculation and thermocouple tools, https://millenia.cars.aps.anl.gov/gsecars/ruby/ruby.htm, accessed August 13, 2020.
[28] G. J. Piermarini, S. Block, and J. D. Barnett, Hydrostatic limits in liquids and solids to 100 kbar, J. Appl. Phys. **44**, 5377 (1973).
[29] CrysAlisPro 1.171.38.46, Rigaku oxford diffraction (2017).
[30] G. Kresse and J. Hafner, Ab initio molecular dynamics for liquid metals, Phys. Rev. B **47**, 558 (1993).
[31] G. Kresse and J. Furthmüller, Efficient iterative schemes for ab initio total-energy calculations using a plane-wave basis set, Phys. Rev. B **54**, 11169 (1996).
[32] P. E. Blöchl, Projector augmented-wave method, Phys. Rev. B **50**, 17953 (1994).
[33] L. Hedin, New method for calculating the one-particle Green's function with application to the electron-gas problem, Phys. Rev. **139**, A796 (1965).
[34] M. S. Hybertsen and S. G. Louie, Electron correlation in semiconductors and insulators: Band gaps and quasiparticle energies, Phys. Rev. B **34**, 5390 (1986).
[35] M. Shishkin and G. Kresse, Implementation and performance of the frequency-dependent *GW* method within the PAW framework, Phys. Rev. B **74**, 035101 (2006).
[36] S. M. Dancoff, Non-adiabatic meson theory of nuclear forces, Phys. Rev. **78**, 382 (1950).
[37] J. Paier, M. Marsman, and G. Kresse, Dielectric properties and excitons for extended systems from hybrid functionals, Phys. Rev. B **78**, 121201(R) (2008).
[38] M. Novak, S. N. Zhang, F. Orbanić, N. Biliškov, G. Eguchi, S. Paschen, A. Kimura, X. X. Wang, T. Osada, K. Uchida, M. Sato, Q. S. Wu, O. V. Yazyev, and I Kokanović, Highly anisotropic interlayer magnetoresistance in ZrSiS nodal-line Dirac semimetal, Phys. Rev. B **100**, 085137 (2019).
[39] K. R. Shirer, K. A. Modic, T. Zimmerling, M. D. Bachmann, M. König, P. J. W. Moll, L. Schoop, and A. P. Mackenzie, Out-of-plane transport in ZrSiS and ZrSiSe microstructures, APL Mater. **7**, 101116 (2019).
[40] W. Zhou, A. N. Rudenko, and S. Yuan, Effect of mechanical strain on the optical properties of nodal-line semimetal ZrSiS, Adv. Electon. Mater. **6**, 1900860 (2019).
[41] T. Habe and M. Koshino, Dynamical conductivity in the topological nodal-line semimetal ZrSiS, Phys. Rev. B **98**, 125201 (2018).
[42] Please note that we concentrate here on the high-energy range, since the temperature dependence of the low-energy optical conductivity for $\mathbf{E}\|ab$ has been discussed in detail in Ref. [14].
[43] It is interesting to note that the temperature-dependent shift of the $L4$ peak slightly changes its slope between 150 and 100 K. In the same temperature range, the temperature dependence of the dc resistivity changes [13] and several Raman modes show an anomaly in their position and width [44], which was attributed to an interplay between electronic and phononic degrees of freedom.
[44] R. Singha, S. Samanta, S. Chatterjee, A. Pariari, D. Majumdar, B. Satpati, L. Wang, A. Singha, and P. Mandal, Probing lattice dynamics and electron-phonon coupling in the topological nodal-line semimetal ZrSiS, Phys. Rev. B **97**, 094112 (2018).
[45] S. M. Young and C. L. Kane, Dirac Semimetals in Two Dimensions, Phys. Rev. Lett. **115**, 126803 (2015).
[46] We cannot completely rule out that the $F2$ peak already exists at ambient pressure, but cannot be resolved due to small oscillator strength and overlap with higher-energy interband transitions.
[47] C. C. Gu *et al.*, Experimental evidence of crystal symmetry protection for the topological nodal line semimetal state in ZrSiS, Phys. Rev. B **100**, 205124 (2019).
[48] D. VanGennep, T. A. Paul, C. W. Yerger, S. T. Weir, Y. K. Vohra, and J. J. Hamlin, Possible pressure-induced topological quantum phase transition in the nodal line semimetal ZrSiS, Phys. Rev. B **99**, 085204 (2019).
[49] F. D. Murnaghan, The compressibility of media under extreme pressures, Proc. Natl. Acad. Sci. U.S.A. **30**, 244 (1944).
[50] B. Salmankurt and S. Duman, First-principles study of structural, mechanical, lattice dynamical and thermal properties of nodal-line semimetals ZrXY (X = Si,Ge; Y = S, Se), Phil. Mag. **97**, 175 (2016).
[51] R. J. Kirby, A. Ferrenti, C. Weinberg, S. Klemenz, M. Oudah, S. Lei, C. P. Weber, D. Fausti, G. D. Scholes, and L. M. Schoop, Transient Drude response dominates near-infrared pump-probe reflectivity in nodal-line semimetals ZrSiS and ZrSiSe, J. Phys. Chem. Lett. **11**, 6105 (2020).
[52] J. Ebad-Allah, M. Krottenmüller, J. Hu, Y. L. Zhu, Z. Q. Mao, and C. A. Kuntscher, Infrared spectroscopy study of the nodal-line semimetal candidate ZrSiTe under pressure: Hints for pressure-induced phase transitions, Phys. Rev. B **99**, 245133 (2019).
[53] M. Krottenmüller, M. Vöst, N. Unglert, J. Ebad-Allah, G. Eickerling, D. Volkmer, J. Hu, Y. L. Zhu, Z. Q. Mao, W. Scherer, and C. A. Kuntscher, Indications for Lifshitz transitions in the nodal-line semimetal ZrSiTe induced by interlayer interaction, Phys. Rev. B **101**, 081108(R) (2020).
[54] L. C. Hebel and C. P. Slichter, Nuclear spin relaxation in normal and superconducting aluminum, Phys. Rev. **113**, 1504 (1959).
[55] We note that the $F1$ peak derives its spectral weight from the high-energy rather than low-energy region. This is opposite to the excitonic insulator scenario, where the spectral weight comes from the Drude peak or low-energy region, in general.
[56] S. Samaneh Ataei, D. Varsano, E. Molinari, and M. Rontani, Evidence of ideal excitonic insulator in bulk MoS_2 under pressure, Proc. Natl. Acad. Sci. U.S.A. **118**, e2010110118 (2021).